npj | materials sustainability

Review

https://doi.org/10.1038/s44296-025-00070-y

Microstructural insights and technical challenges of effectively adopting high-volume GGBS in blended cements for low-carbon construction

Check for updates

Zengliang Yue[1] & Xiaohong Zhu[1,2] ✉

High-volume blended slag cements (HVBSC), with over 70% GGBS replacement, offer a promising route to reduce clinker use and utilise industrial by-products. This review examines HVBSC hydration mechanisms, reaction products (C-(A)-S-H, LDH), strength development, and durability challenges. Strategies to enhance early-age performance are discussed, alongside the need for multiphysics modelling. A conceptual framework is proposed to guide HVBSC development and scaling in suitable regional contexts.

Cement production is a major contributor to global anthropogenic CO_2 emissions, accounting for approximately 8–9% of total emissions and 2–3% of global energy consumption[1]. The majority of these emissions arise from the calcination of limestone at temperatures reaching up to 1450 °C, as well as the combustion of fossil fuels[2]. As illustrated in Fig. 1a, global cement production has exhibited a consistent upward trend from 1995 to 2023. China, the world's largest cement producer, has maintained an annual output exceeding 2000 million metric tonnes (Mt) since 2010, reaching a peak in 2014 driven by extensive infrastructure development. However, production has declined in the years since, likely reflecting China's strategic transition towards carbon neutrality[3], partly through the incorporation of industrial wastes and by-products into low-carbon cement formulations[4,5]. In addition, the country's mature stage of industrialisation and urbanisation has shifted priorities from large-scale construction to the maintenance and repair of existing infrastructure[6,7].

India, by contrast, has experienced a marked increase in cement production since 2003, with output nearly quadrupling by 2023. This growth is primarily driven by rapid population expansion and accelerated urbanisation[8], which have significantly increased the demand for cement-based infrastructure. Beyond China and India, the European Union (EU) is the third-largest cement producer globally, maintaining relatively stable production levels of around 180 Mt per year since 2015. In general, cement demand in developed nations remains stable and comparatively low, whereas developing countries continue to exhibit rising demand aligned with ongoing urban development and infrastructure expansion.

Over the past several decades, substantial efforts have been devoted to mitigating the environmental impact of cement production through the partial replacement of Portland cement with supplementary cementitious materials (SCMs)[9,10]. Among these, ground granulated blast furnace slag (GGBS), a by-product of the pig iron industry, has emerged as a particularly promising candidate due to its amorphous structure and latent hydraulic reactivity[11]. In this paper, unless otherwise stated, the term *slag* refers to GGBS and to blended slag cements composed primarily of GGBS in combination with Portland cement or clinker. Life cycle assessments have demonstrated that substituting Portland cement with GGBS can reduce greenhouse gas emissions by approximately 47.5%[10], contributing to an overall environmental impact reduction of up to 30%[12]. As a result, blended slag cements have gained widespread use in structural applications[13–15]. According to BS EN 197-1[16], Portland–slag cements are categorised as CEM II/A-S and CEM II/B-S, which contain 6–20 wt.% and 21–35 wt.% slag, respectively. Blast furnace cements, designated as CEM III/A, III/B, and III/C[16], contain slag substitution levels of 36–65 wt.%, 66–80 wt.%, and 81–95 wt.%, respectively. These represent the highest permitted clinker replacement levels, with substitutions exceeding 60 wt.% and 80 wt.% commonly referred to as high-volume and ultra-high-volume blended slag cements (HVBSCs), respectively.

Despite variability in GGBS reactivity depending on source material[17], iron manufacturers typically produce slag with relatively consistent physicochemical properties due to standardised blast furnace operations[18–20]. For every tonne of pig iron produced, approximately 260–300 kg of slag is generated[21]. Figure 1b, c illustrates global trends in pig iron and crude steel production from 1995 to 2023. As of 2023, China remains the dominant global producer of GGBS, accounting for roughly 67% of worldwide output, with an estimated annual production of 227–261 Mt. Since 2018, global GGBS production has stabilised in the range of 338–390 Mt per year. Carbon steel is produced in either a basic

[1]Key Laboratory of Urban Security and Disaster Engineering of Ministry of Education, Beijing University of Technology, Beijing, China. [2]Department of Civil and Environmental Engineering, University of California, Berkeley, CA, USA. ✉e-mail: xiaohong.zhu@berkeley.edu; xiaohong.zhu@bjut.edu.cn

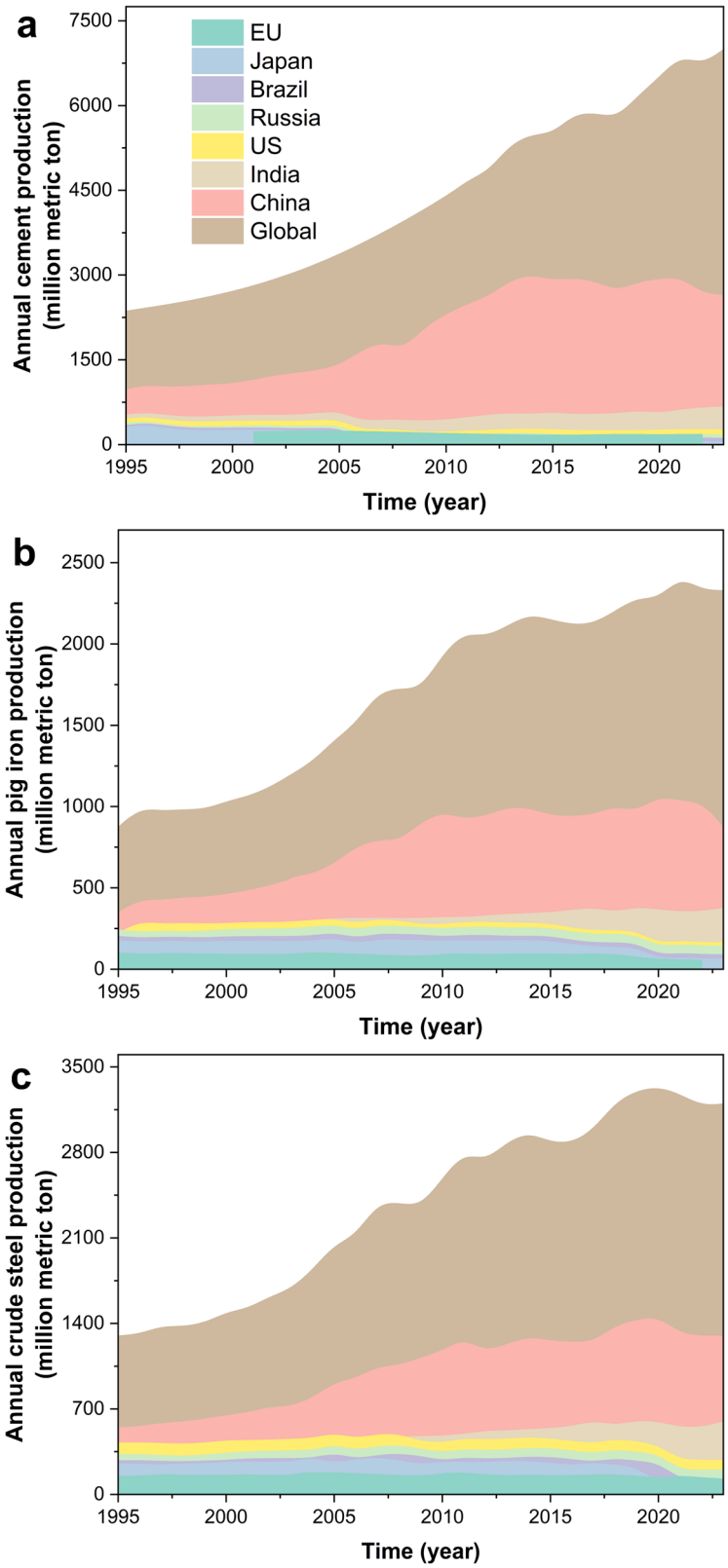

Fig. 1 | Annual production of Portland cement, pig iron and crude steel from 1995 to 2023 in selected main countries and regions. a Portland cement, **b** pig iron and **c** crude steel. Datasets originated from the China National Bureau of Statistics[167], U.S. Geological Survey[168], Statista[169], Cembureau[170] and EUROFER (European Steel Association)[171].

oxygen furnace (BOF), an electric arc furnace (EAF) or a ladle furnace (LF)[22]. China, as the world's largest producer of both pig iron and crude steel, has maintained production levels of approximately 900 Mt/year and 1000 Mt/year, respectively, since 2020. Although a slight post-2020 decline is observed, China's output remains substantially higher than that of any other nation, approximately eight times higher for pig iron and five times higher for crude steel.

The pig iron sector continues to seek sustainable avenues for utilising slag by-products in value-added applications[23–25]. India exhibits a similar upward trajectory in pig iron and crude steel production, aligned with growing infrastructure demands. Meanwhile, the European Union, historically a major iron and steel producer[26], has stabilised at annual outputs of approximately 90 Mt for pig iron and 150 Mt for crude steel. While the EU has made considerable progress in adopting GGBS for blended cements, slag

utilisation remains even more critical in Asia (e.g., China, India, Japan) and the Americas (e.g., USA, Brazil), where iron production volumes remain high. Considering producing low-carbon cements and achieving the United Nations' sustainable development goals, SDG9 ("build resilient infrastructure, promote inclusive and sustainable industrialisation and foster innovation")[27], huge GGBS production capacity worldwide means that it is essential to develop cements with ultra-high contents of GGBS (over 70 wt.% replacement).

Steel slag, a by-product comprising 15–20 wt.% of total steel production[28,29], includes BOF slag, EAF slag, and LF slag[30]. Its effective management is critical for advancing industrial waste valorisation and circular economy strategies. Given the scale of global crude steel production (Fig. 1c), innovative utilisation of steel slags in cement and concrete applications is increasingly important. Among these, BOF slag exhibits higher reactivity and can replace up to 20 wt.% of Portland cement[28]. However, significant knowledge gaps remain regarding both the fundamental behaviour and practical implementation of steel slag in infrastructure. Although steel slag cements are not the central focus of this study, they represent a promising avenue for future research. For further technical developments, see the reference[22].

This paper provides a critical review of recent advances in understanding the reaction mechanisms of high-volume blended slag cements (HVBSCs), with particular emphasis on hydration products and strength development. Strategies to accelerate early-age kinetics and improve mechanical performance are examined in detail. Given the pivotal role of durability in structural longevity, the paper also evaluates the durability performance of HVBSCs and highlights the limitations of conventional testing methods. Finally, a conceptual framework for future directions is proposed to facilitate the industrial-scale adoption of HVBSCs.

Reaction mechanism of high-volume blended slag cements (HVBSC)

Figure 2a–c presents the thermodynamic modelling of blended slag cements at 28 days of curing, where the slag replacement of clinker is increased from 10 wt.% to 95 wt.%. Modelling indicates the formation of C-(A)-S-H gel, portlandite, ettringite, monosulphate/monocarbonate aluminates due to the presence of calcite in the clinker and Mg-Al-OH-LDH, which are consistent with experimental results[31,32]. Although iron-siliceous hydrogarnet is normally reported to form under elevated temperature and long-term age[33,34], synchrotron X-ray absorption spectroscopy (XAS) reported its formation at room temperature after 1 day's hydration in Portland cement[35]. Strätlingite is unstable in the presence of Portlandite[36], which has been reported to form in high-alumina cements[37] and calcium sulphoaluminate cements[38]. However, direct experimental evidence for the formation of strätlingite and hydrogarnet in high-volume or ultra-high-volume slag-blended cements remains limited. Although thermodynamic modelling predicts their stability based on the principle of minimum Gibbs free energy, experimental observations are inherently made under non-equilibrium conditions, particularly during early hydration stages. This temporal mismatch between equilibrium predictions and kinetic processes likely accounts for the observed discrepancies. Additionally, if the as-formed crystals of Al-bearing hydration products are not large enough, their signals may be invisible in traditional lab-based techniques such as XRD or TG.

Figure 2d presents the XRD pattern of ultra-high volume blended slag cements with 90 wt.% slag replacement after 2 years of curing, using three different blast furnace slags sourced from pig iron plants in China. The presence of portlandite in all three slag-based pastes (Fig. 2d) suggests that the conventional pozzolanic reaction between $Ca(OH)_2$ and aluminosilicate materials in blended cement systems[39] may not adequately explain the reaction mechanism in ultra-high volume blended slag cements. The incomplete reaction of alite and belite after 2 years in these mature paste samples is likely due to the minor amount of clinker and the latent hydraulic properties of slag, where the alkalinity/pH level (as indicated in Fig. 2c) in the pore solution is insufficient to fully dissolve the clinker and aluminosilicate materials. Additionally, it should be noted that only part of the clinker particles can be dissolved, as the reaction products surround the particle hindering particle dissolution and restricting the completed hydration[40,41].

Additionally, a minor amount of strätlingite was observed only in the GGBS2-based pastes (Fig. 2d), which contradicts the thermodynamic modelling results shown in Fig. 2a. This discrepancy is mainly attributed to the influence of slag composition on the dissolution rate of elemental species[42,43], setting time[44], microstructure[45,46] and cements' performance[46,47]. Solely relying on XRF (X-ray fluorescence) results as input in thermodynamic modelling and defining the reactivity of slag, basicity coefficient $(\frac{\omega_{CaO}+\omega_{MgO}}{\omega_{SiO_2}+\omega_{Al_2O_3}})$ or activity coefficient $\frac{\omega_{Al_2O_3}}{\omega_{SiO_2}}$, may not be sufficient to accurately picture the true reactivity of slag and predict the phase composition of hydrated pastes. Although the R^3 (rapid, relevant and reliable) test is a popular method for assessing the pozzolanic reactivity of SCMs[48–50], the recommended 40 °C, used to mimic the reacting environment with cement, and 7 days of testing duration might not truly reflect the real reaction conditions in high-volume blended slag cements due to latent hydraulic properties of slag and ambient temperature due to dilution of cement[17]. The criteria for determining slag reactivity remain a subject of ongoing research and debate. Notably, a consistently strong correlation between amorphous content and slag reactivity, or the resulting strength development, has not been established[51]. Recent studies have begun to suggest that slag reactivity may be more closely linked to the coordination state of aluminium (i.e., tetrahedral, pentahedral, or octahedral)[42,52–54], particularly the ratio of Al[IV] to Al[V]. However, further investigation is needed to elucidate these relationships and fully understand the underlying mechanisms.

Although thermodynamic modelling predicts only the formation of C-S-H gel due to limitations in the available database, extensive studies have reported and confirmed that the aluminium content from slag tends to substitute the bridging sites of silicon tetrahedra, forming $Q^2(1Al)$ and resulting in aluminium-substituted calcium silicate hydrate (C-(A-)S-H). The maximum aluminium substitution[31,55,56], as described, the Al/Si ratio, is ~0.2 representing a practical maximum in Portland cements blended with aluminosilicate-rich supplementary materials[57,58].

After 60 wt.% slag substitution (Fig. 2a), which is typically considered high-volume blended slag cement, the reduced clinker content leads to decreased levels of calcium and sulphur in the pore solution (Fig. 2b), resulting in a reduction of ettringite and the formation of monosulphate. However, as the slag content increases further, the volume of ettringite rises again after 85 wt.% replacement due to the increased SO_3 content provided by the slag. It should be noticed that most of the sulphur species in the slag are in reduced form[59,60]. However, thermodynamic modelling alone cannot fully resolve this issue, as the GGBS composition is typically derived from bulk XRF analysis, which only provides the elemental oxides and overlooks the speciation of key elements. This limits the ability to accurately represent the reactive phases and potential reaction products.

Figure 2c shows the Ca/Si ratio of C-S-H gel and the pH value in the pore solution of blended slag cement, where Portland cement is gradually replaced by slag. Increased slag substitution leads to a decrease in both the Ca/Si ratio and pH value, corresponding to the reduction in clinker content. The change in the Ca/Si ratio of C-S-H gel is consistent with experimental observations[61]. A significant decrease in pH value is observed when slag replacement exceeds ~70 wt.%. This reduced pH weakens the slag reactivity, which in turn results in a longer setting time[62,63], lower compressive strength[64–66] and lower degree of slag reaction[51,67,68] in the first 28 days of curing, compared to neat Portland cement. Therefore, when adopting ultra-high volume blended slag cements, where slag substitution exceeds 80%, it is essential to expect an increase of the sulphur and aluminium contents in the pore solution, as shown in Fig. 2b. The release of these two elements could promote the formation of sulphur-bearing phases such as ettringite and Ca-Al-LDH/Mg-Al-LDH (layered double hydroxide). This reduction in aluminium content in the pore solution, originating from the GGBS, is particularly important because it can enhance the dissolution of glassy blast furnace slags, thereby accelerating slag hydration[69,70].

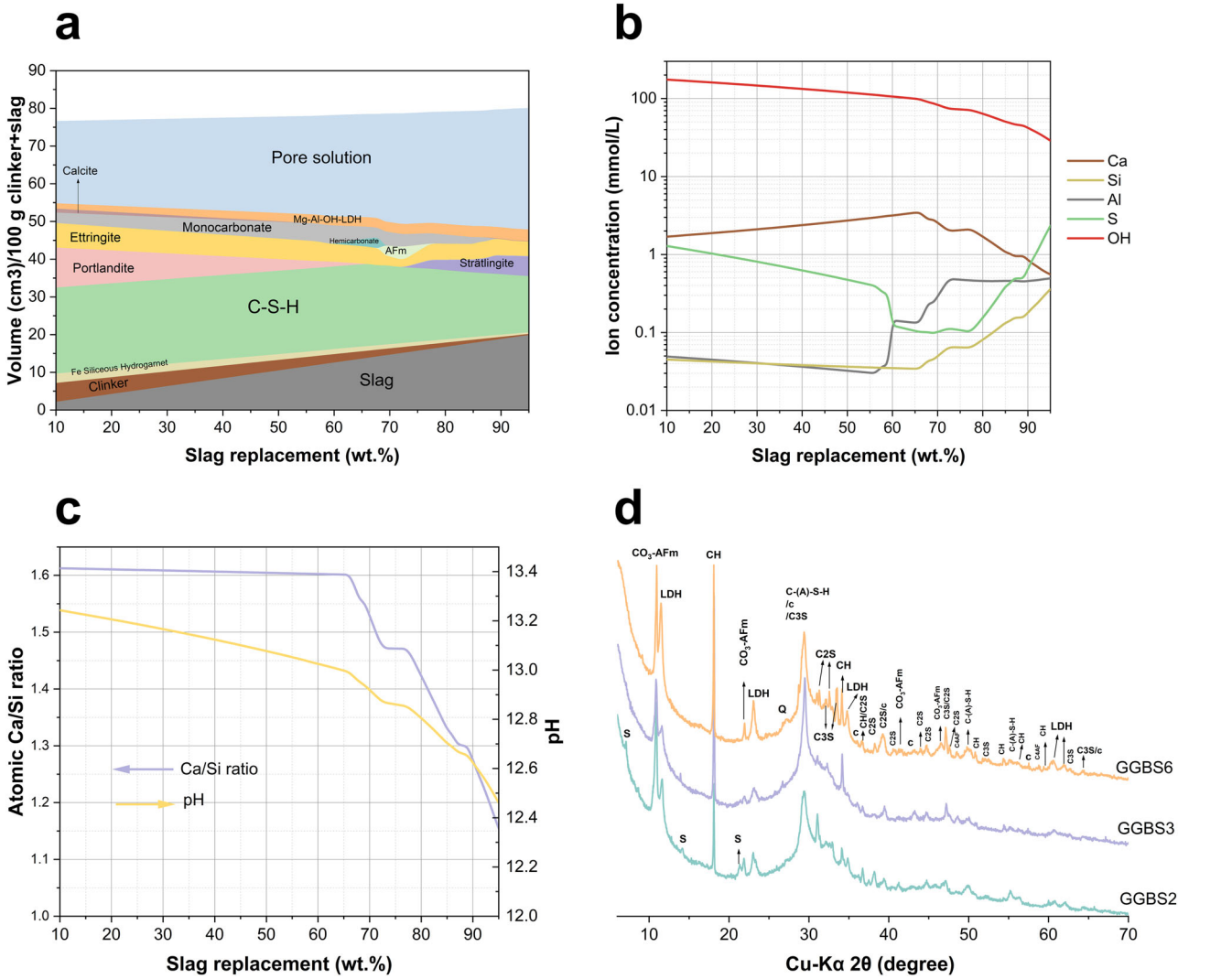

Fig. 2 | Thermodynamic modelling in blended slag cements for 28 days of hydration. a Phase assemblage of blended slag cements with increased slag replacement from 10 to 95%. **b** Pore solution chemistry in blended slag cements; Mg concentration is excluded due to its very low concentration below 1E-6 [mmol/L]. **c** Atomic ratio of Ca/Si ratio in C-S-H gel and pH value in the pore solution with increased slag substitution. Thermodynamic modelling is based on the software package GEM-Selektor v.3 (GEMS3)[172,173] using the latest database Cemdata 18.1[174]. The degree of clinker reaction is assumed to be 80% at 28 days, based on MPK model[175]. DoR of alite (i.e., impure C_3S), belite (i.e., impure C_2S), aluminiate and ferrite at 28 days are 85%, 55%, 83% and 63%, respectively. The summation of those four unreacted phases is assigned to the clinker in 2a. The degree of GGBS reaction is assumed to be 40 wt.% at 28 days, based on the model from Kolani et al.[68]. Clinker and slag compositions are adopted from[31,176]. **d** XRD patterns of ultra-high volume blended slag cements (90 wt.% GGBS and 10 wt.% cement) using GGBS2, 3 and 6 after 2 years of seal curing. Information about those three slags is referred to[44]. CO_3-AFm-monocarboaluminate (PDF#00-041-0725); LDH-hydrotalcite-type phase (PDF#01-089-0460); C-(A-)S-H-aluminium substituted calcium silicate hydroxide (PDF#00-006-0010); CH-portlandite (PDF#00-004-0733); S-Strätlingite (PDF#00-029-0285); C_3S-representative alite(PDF#01-073-2077); C_2S-representative belite(PDF#00-033-0303); C_4AF-ferrite (PDF#98-009-8832).

Microstructure evolution and mechanical properties

C-(A)-S-H nanostructure and formed layered double hydroxides (LDH) phases

The releasing of aluminium from GGBS is crucial for forming C-(A)-S-H as illustrated in Fig. 3a. The formation of bridging tetrahedra (BT) between the paired tetrahedra (PT) enables the lengthening in the (alumino)silicate chain, where [AlO_4] was proven to only replace (or occupy) the BT position[71], forming a chain with a maximum Al/Si ratio that depends on the chain length and available BT positions. In this regard, the [AlO_4] cannot be freely inserted into the silicate chain but depends on the chain length (i.e., available BT positions). Insertion of [AlO_4] and the increased chain length will gradually change the fibrillar-like C-(A)-S-H to the foil-like, as observed in a 60 wt.% slag blended cement hydrated from 14 days to 28 days in Fig. 3b. The chemical composition of C-(A)-S-H in slag-blended cement is plotted in Fig. 3c, with an arrow showing the trend of increasing slag content. Regardless of the hydration time, the Al/Ca ratio in C-(A-)S-H depends on the slag content in the blend, where there is a general trend (the average values are given in Fig. 3d) between Al/Ca ratio and Si/Ca ratio in as-formed C-(A)-S-H. It means that the Ca/Si ratio of C-(A-)S-H can be linked with the mean chain length in the blend, corresponding to a maximum Al replacement ratio in the gel. An important question to address is whether the composition of GGBS also hugely influences the Ca/Si ratio of the C-(A)-S-H that forms. The answer to this question will determine the structural and compositional characteristics of C-(A)-S-H, following the general trend (Fig. 3d) observed, which should be the universal relationship of C-(A)-S-H in GGBS blends.

Figure 4a presents the Ca/Si and Al/Si ratios of C-(A)-S-H gel as a function of slag replacement (wt.%) after 20 years of hydration. The Ca/Si ratio decreases with increased slag content, primarily due to the dilution of Portland cement and reduced slag reactivity[41]. In contrast, higher slag replacement promotes Al substitution in the bridging sites of silicon tetrahedra[58,71–73], as shown in Fig. 3a. The reduction in Ca/Si, particularly

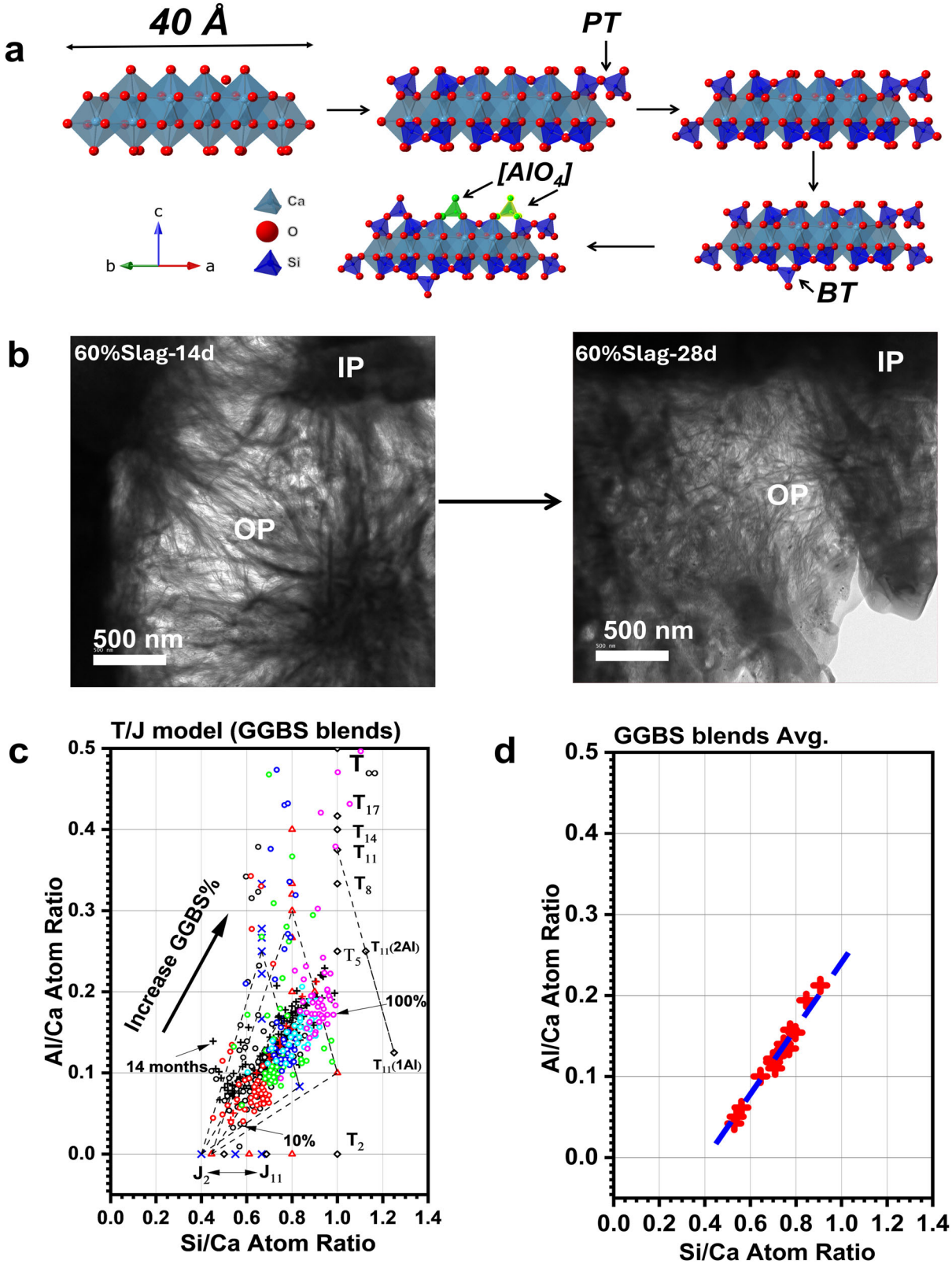

Fig. 3 | Nanostructure and chemical composition of C-(A)-S-H gel in high-volume blended slag cements. a Formation process of C-(A)-S-H from the [CaO] polyhedral to linear Tobermorite-like structure; **b** morphological changes of C-(A)-S-H in 60 wt.% slag-blended cement observed by TEM (Transmission Electron Microscopy), images reproduced from[56]; **c** chemical composition determined by TEM-EDX (Energy Dispersive X-Ray Spectroscopy) and structural similarities of C-A-S-H in slag blended cement with the increasing content of slag, full information of the data points can be found in[56]; **d** the universal relationship between the Si/Ca ratio and Al/Ca ratio of C-(A)-S-H in slag blended cements.

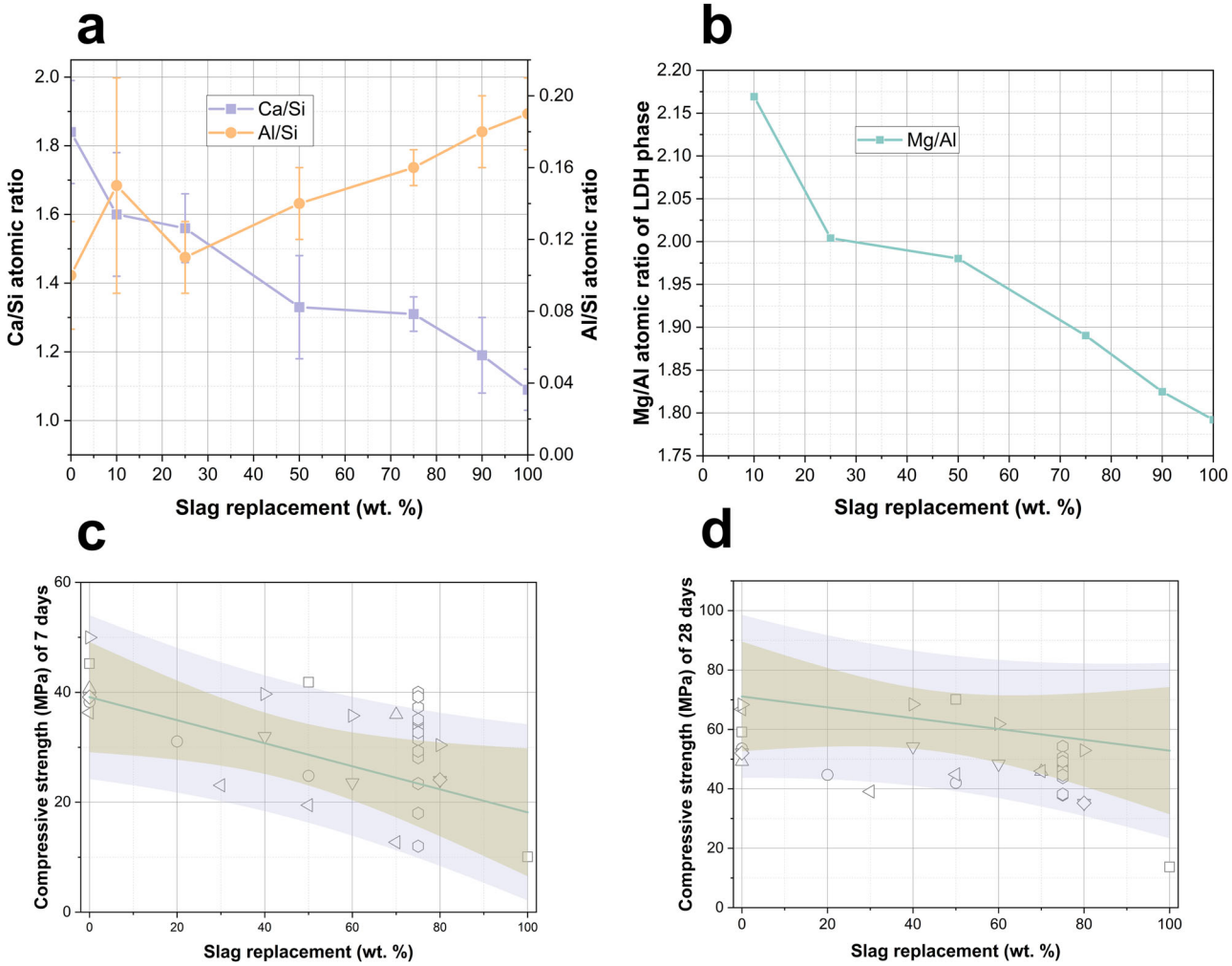

Fig. 4 | Ca/Si and Al/Si atomic ratio of C-(A-)S-H, Mg/Al atomic ratio of LDH phase, compressive strength of 7 days and 28 days cured mortars, as a function of slag replacement. a Ca/Si and Al/Si atomic ratios of C-(A-)S-H gel and **b** Mg/Al atomic ratio of Mg-Al-LDH phase after 20 years of hydration as a function of slag replacement (wt. %). The chemical composition of C-(A-)S-H gel and Mg-Al-LDH phase were determined by TEM-EDX in ref. 41. **c** 7 days' compressive strength and **d** 28 days' compressive strength in blended slag cements mortar, as a function of slag replacement (wt. %). Data in 4c and 4 d is sourced from published literature; the symbols are referred to as square[177], circle[178], upward triangle[64], downward triangle[179], diamond[180], left-pointing triangle[65], right-pointing triangle[181], and hexagon[17]. In Fig. 4c, d the light beige band indicates the 95% confidence interval, providing a range within which the true parameter values are expected to fall with 95% certainty. Similarly, the light blue band represents the prediction interval, showing the expected range for future data points. Both intervals visually convey the level of uncertainty and variability in the data, with the bands narrowing as the model fits the data.

after 30 wt.% slag replacement, results in similar Ca/Si ratios in both inner (initially containing unreacted clinker and GGBS) and outer (initially filled with water) reaction products[61]. This behaviour contrasts with pure Portland cement systems, where the Ca/Si ratio is consistently higher in inner products due to the presence of portlandite[74,75] but resembles clinker-free alkali-activated slag cements[76,77].

As GGBS replacement increases, the decreasing Ca/Si ratio and increasing Al/Si ratio in outer reaction products progressively alter the morphology of the primary binding gel, which constitutes over 60 wt.% in HVBSC, as shown by the thermodynamic calculation in Fig. 2a. The structure shifts from a linear, fibrillar morphology at slag replacement levels below 30 wt.% to a fine, foil-like nanostructure at higher GGBS content (see Fig. 3b as an example of changing)[41,56,61]. The foil-type nanostructure may help to reduce the diffusivity of the pastes and increase durability performance, which will be discussed in the following section.

Mg-Al-LDH (layered double hydroxides) is a crucial phase in cementitious materials due to its ability to absorb and exchange ingress ions such as carbonate[78,79], sulphate[80] and chloride[81–83], helping to maintain the integrity of the matrix. The Mg-Al-LDH phases are derived from layered double magnesium hydroxide, where a portion of Mg^{2+} is substituted by Al^{3+}, creating a + 1 charge on the main layer. This charge is balanced by anions in the interlayer regions, which also contain water molecules[84]. The intercalated anionic group are various including OH^-, called meixnerite ($Mg_6Al_2(OH)_{18}•2H_2O$), Cl^-, NO_3^-, CO_3^{2-} and SO_4^{2-}[85,86].

Figure 4b shows a decrease in the Mg/Al ratio of the Mg-Al-LDH phase in the inner reaction product regions with increasing slag content after 20 years of hydration. This phase predominantly precipitates in these inner regions, as Mg^{2+} dissolves minimally and is not significantly transported to the outer reaction zones[61,87]. The Mg/Al ratio drops below 2 after 25 wt.% of slag replacement, which is lower than hydrotalcite ($Mg_6Al_2(OH)_{16}CO_3•4H_2O$) or the minimum value of 2 in quintinite ($Mg_4Al_2(OH)_{12}CO_3•3H_2O$)[88]. This decrease is likely related to a poorly ordered $Al(OH)_3^-$ based layered structure intercalated within the Mg-Al-LDH interlayers[41,89]. However, direct evidence regarding the crystallographic structure of this LDH phase in HVBSC remains lacking.

Development of compressive strength

Figure 4c, d illustrates the compressive strength development in blended slag cement mortars after 7 days (Fig. 4c) and 28 days (Fig. 4d), based on data

from the literature. At 7 days of curing, a linear relationship is observed: increasing slag replacement reduces compressive strength. This is primarily due to the dilution of clinker and the lower degree of slag reactivity due to reduced pH value in the pore solution (Fig. 2c) at early stages[68]. However, after 28 days of curing, the linear strength trend becomes less distinct, and the compressive strength of plain Portland cement mortar becomes comparable to that of high-volume blended slag cement (HVBSC) with 60 wt.% slag replacement, provided that the GGBS composition is appropriately tailored[17]. This suggests that the latent hydraulic properties of GGBS and its chemical composition contribute significantly to the degree of reaction at later ages (28 days)[90–92], with OH^- ions from GGBS dissolution facilitating the ongoing hydration process[42]. Figure 4d highlights the potential feasibility of HVBSC for load-bearing applications when curing is extended to 28 days. The reaction kinetics and degree of reaction in HVBSC can be enhanced by adding chemical additives and optimising mix design and grinding procedures—topics that will be explored in the following section.

Perspective and challenges in high-volume blended slag cements (HVBSC)

Although slag replacements below 50% have been successfully adopted in industrial applications, particularly in marine structures[13], higher substitution levels of 70–90% remain largely confined to laboratory research. Optimising setting time, reaction kinetics, and mechanical performance remains essential and must be tailored to both the slag composition and site-specific curing conditions. Moreover, the long-term durability of such systems is not yet well understood. This section does not aim to comprehensively address all aspects of HVBSCs, such as additive types, durability under carbonation, sulphate and chloride exposure, or GGBS compositional variability, but rather to highlight key challenges and outline promising directions for future research and development.

How to increase reaction kinetics in HVBSC?

The major barriers to using blended slag cements with over 70 wt.% replacement are the longer setting time, lower early strength (e.g. first 7 days), and reduced degree of reaction compared to Portland cement binders. The dilution of clinker slows both cement and slag reactions, primarily due to the lack of sufficient hydroxide ions (i.e., low pH, see Fig. 2c) to break down the glassy structure of the slag. To address these challenges, various additives have been explored, including sodium hydroxide[93,94], sodium silicate[95], sodium sulphate[67,96], calcium sulphate[97,98], calcined layered double hydroxide (CLDH)[99,100] and sodium bicarbonate[101]. Additionally, raising the curing temperature up to 40 °C[65] has been used to accelerate early-stage reactions and enhance early strength. However, the long-term understanding of phase assemblage and microstructure in HVBSC remains largely unknown.

As discussed in Section "Reaction mechanism of high-volume blended slag cements", increased cement substitution leads to a reduction in the amount of main binding gel, i.e., C-(A)-S-H, along with a decreased degree of reaction in both cement and slag, primarily due to the lower pH value in the pore solution and higher Ca concentration released by slag that can limit the dissolution of clinker[56]. To enhance reaction kinetics in the early stages (e.g. first 3 days), it is essential to accelerate the dissolution of both cement and slag, thereby increasing the formation of reaction products, reducing setting time and improving early strength development. At replacement levels below 50 wt.%, the hydration of clinker plays a dominant role during this period. Consequently, the observed reduction in early strength is primarily attributed to the decreased cement content and increased proportion of supplementary materials, which together lead to a lower yield of C-(A)-S-H gel required for sufficient mechanical performance. Improving clinker reactivity in the early stages can be achieved through increasing fineness[102], optimising clinker composition (i.e., increase the content of M-type alite or aluminates)[103], and sulphate adjustment[104]. However, the limited clinker content in HVBSC may suggest different hydration mechanisms as indicated in Section "Reaction mechanism of high-volume blended slag cements" that portlandite is not sufficient to activate the GGBS. Therefore, additional parameters and levers are required within the HVBSC system to promote reaction kinetics effectively.

Significant efforts have been made over the past decades to enhance reaction kinetics in HVBSC. Beyond the use of chemical activators, employing fillers and controlling particle size are crucial strategies for replacing clinker and promoting reaction kinetics in HVBSC. Limestone, both a primary raw material in clinker production and a by-product of quarrying, is among the most ubiquitous materials used in cementitious systems. It has been incorporated into cement formulations for decades[105] and is standardised as a supplementary component for Portland cement replacement worldwide[106]. Substituting a significant amount of Portland cement with limestone increases the relative water/cement ratio, creating more space for clinker particles to hydrate[107]. Limestone acts as a nucleation site, with its particle surface exhibiting a strong affinity for calcium ions, thereby promoting the formation of C-S-H gel[108]. Additionally, limestone can react with aluminates to form mono/hemi carbon-aluminates and stabilise ettringite, which enhances the degree of reactions[109,110].

In Portland cement-limestone-slag cements, finely ground limestone[111] can replace up to 20 wt.% of cement in a 50 wt.% blended slag cement system, effectively enhancing both clinker and slag hydration as well as compressive strength, with approximately 30 wt.% of the limestone reacting after 180 days of curing[31]. However, the feasibility of using limestone in systems with over 70% slag substitution remains uncertain, such as the heterogeneities in particle size distribution. Therefore, attempts can be made by using limestone powders with various fineness.

In addition, particle packing presents a promising approach for increasing cement replacement by optimising the particle size distribution of solids and minimising initial porosity based on the Compressible Packing Model (CPM)[112]. Given that the additives (such as limestone, silica fume, and ultra-fine fly ash) show significant differences in terms of particle size, these powder materials should be carefully optimised and well-mixed with slag according to CPM design before use.

Minor chemical additives, like sulphate, chloride and nitrate salts, are often incorporated into concrete to enhance early strength (e.g. first 28 days)[93,113,114]. Among various accelerators, sodium sulphate is particularly effective in increasing reaction kinetics and early strength development by generating sodium hydroxide in the pore solution and boosting ettringite formation[67,91,93]. Additionally, the use of nanoparticle accelerators is a popular field of research due to their large specific surface area, nucleation effects, and potential pozzolanic activity. C-S-H seeds, with controlled particle size and Ca/Si ratio, have been reported to significantly enhance the extent of reaction and strength development[115–118]. However, challenges such as low reactivity at low temperatures[119] and potential nanoparticle agglomeration in poorly controlled systems[120] may necessitate increased water content and/or the use of superplasticisers. However, it is important to note that most commercially available C-S-H seed products are specifically formulated to mitigate these issues, and their successful application in accelerating the hydration of GGBS has been well-documented[121]. In this context, the use of accelerators (multi-salts, small amounts of alkaline, or nano-seeds) in HVBSC is considered a possible pathway for early hydration enhancement.

Other carbon nanoparticles, such as graphene-based materials (GMs) and carbon nanotubes (CNTs), have garnered considerable attention in the fields of cement and concrete. Studies have demonstrated that incorporating small amounts of these nanomaterials can enhance mechanical properties, including Young's modulus, compressive and flexural strength, and thermal conductivity[122–125]. While the use of GMs and CNTs may contribute to reducing the carbon footprint and improving sustainability in cement and concrete production[126], the significantly higher costs associated with their production, transportation, and storage[127,128] present a philosophical and practical contradiction to the inherently low-cost nature of cement. For that reason, the carbon in concrete cannot only serve as the accelerator but also as conductive media, aiming to provide additional signals for structural monitoring[129,130].

The following strategies may effectively enhance the early-age hydration of HVBSC: (a) incorporating finely ground limestone as a partial slag replacement to optimise particle packing, provide nucleation sites, and promote the formation of CO_3-AFm phases; (b) introducing minor chemical additives to elevate the pore solution pH, thereby accelerating the reaction kinetics of both clinker and slag; and (c) employing nanoparticles, such as C–S–H seeds, graphene-based materials, or carbon nanotubes (CNTs), to stimulate nucleation, enhance pozzolanic reactivity, and improve electrical conductivity.

How to evaluate the durability performance of HVBSC?

Using blended slag cements offers significant benefits in resisting mass transport-related durability issues, including chloride and sulphate attacks. For instance, a 70 wt.% slag replacement can substantially increase service life by reducing the chloride diffusion coefficient by approximately two orders of magnitude compared to plain ordinary cement after 8 years of exposure to a chloride-rich environment[131]. The superior chloride resistivity provided by GGBS has been widely demonstrated, with substitution levels reaching up to 80 wt.%, a figure much higher than that achievable with other pozzolanic materials, depending on engineering requirements, both in laboratory settings and onsite applications[13].

Blending slag with Portland cement also enhances sulphate resistivity. Increased slag content reduces the amount of portlandite, thereby mitigating the formation of gypsum and expansive ettringite, which helps prevent crack formation and instability in the cement matrix[132–134]. However, the composition of slag, which varies depending on the iron manufacturing process, particularly in terms of MgO and Al_2O_3 content, also influences reaction kinetics[17,135], compressive strength[45,65] and durability performance in blended slag cements. This includes resistance to carbonation[79,136], chloride ingress[137,138] and sulphate attack[139,140].

CO_2 dissolves in the pore solution, forming carbonic acid, which then reacts with hydration products in cementitious materials, a process known as carbonation[141,142]. Carbonation induces changes in the mineralogical composition and microstructure, potentially leading to instability in the cement matrix and increased porosity, depending on the mix design and exposure conditions[143,144]. It is one of the primary deterioration mechanisms in reinforced concrete structures, where a reduction in pore solution pH due to carbonation, compromises the stability of the passive film on steel reinforcement. When combined with chloride ingress, this breakdown can ultimately initiate and accelerate corrosion under favourable conditions[145]. Although carbonation typically progresses slowly over the course of a structure's service life, rising atmospheric CO_2 levels and the increasing use of low-carbon cements with reduced clinker content may accelerate the process. HVBSC may be particularly vulnerable, due to their lower pore solution pH (Fig. 2c), reduced quantities of reaction products, especially portlandite, and potentially higher total porosity arising from a lower degree of hydration compared to Portland cement systems. These factors collectively increase the risk of steel reinforcement corrosion. However, on the other hand, the major secondary phase, LDH, resulting from the hydration of slag, shows a significant effect on fixing CO_2 in their interlayers[78,146,147]. Therefore, the remaining questions for HVBSC should be whether carbonation with potential steel corrosion is worse than conventional concrete and if so, how to prevent or delay such a durability issue.

There is no consensus on how to evaluate the carbonation performance of blended slag cements, primarily due to the lack of standardised carbonation testing protocols for high-volume (over 60 wt.%) and ultra-high volume (over 80 wt.%) blended slag cements. Factors such as CO_2 concentration[148,149], temperature[150,151] and relative humidity[152,153] significantly influence the microstructure and measured carbonation depth in these cements. As a result, the use of different carbonation standards in published studies makes it difficult to compare experimental results.

Across the literature, CO_2 concentrations between 1 and 3% (v/v) are generally considered sufficient to induce microstructural changes[154], comparable to those observed under natural carbonation conditions in slag replacement cements below 70 wt.%[148,155]. However, there has been less focus on carbonation in replacement levels above 70 wt.% due to the typically inferior mechanical properties of these cements compared to neat Portland cements and blends with less than 50 wt.% replacement. The recent RILEM TC 281-CCC has emphasised that natural carbonation is more appropriate for evaluating the carbonation performance of HVBSC[154] and detailed carbonation mechanisms in SCMs-based cement systems are referred to[155,156].

HVBSC is not a universal solution to all durability challenges. In fact, incorrect usage and a lack of understanding of slag chemistry, given the diverse physicochemical properties of slags, can lead to adverse outcomes. Concrete degradation often goes unnoticed until visible defects appear in infrastructure, at which point costly remedial work may be required. Therefore, accurate life service models are essential for timely maintenance interventions to prevent such issues. In addition, the so-called "early-age" (for example, before 28 days) durability issues will also be a challenge for HVBSC due to their slow hydration process. The carbonation, chloride ingress and sulphate attack will start much earlier than conventional concrete if the curing is not sufficient.

However, due to the latent hydraulic properties of slag, current modelling methods used to predict cement reaction kinetics, mass transport, and service life in Portland cement systems cannot be directly applied to HVBSC. Substitutions exceeding 70 wt.% essentially transform the system into something closer to clinker-free alkali-activated slag cements (AASC). This suggests that life service models developed for AASC, although still in their early stages, could potentially be adapted for use in high-volume and ultra-high-volume blended slag cements.

In general, durability concerns are central to the longevity of HVBSC. Comprehensive research into the underlying mechanisms, coupled with the development of appropriate testing standards, is essential to reach a consensus within the academic and engineering communities. Given the multi-physics nature of these challenges, encompassing thermo-hydro-mechanical-chemical (THMC) interactions, simplified diffusion models may not provide accurate predictions. A deeper understanding of various durability factors is crucial for formulating robust mathematical equations, which form the basis for developing multi-physics models to accurately predict the service life of HVBSC.

What prospects for furthering sustainability and standardisation of HVBSC?

HVBSC offer significant potential to improve the sustainability of cementitious materials by incorporating by-products from pig iron and steel production as partial replacements for Portland cement, thereby substantially reducing the carbon footprint of construction. It is also important to recognise that GGBS is a regionally sourced material. In areas located near iron and steel production facilities, the use of GGBS can be maximised through optimised mix design strategies. However, in regions without such industries, where the cost of GGBS may approach or exceed that of Portland cement, locally available natural pozzolans may offer a more viable and sustainable alternative. Additionally, high-volume GGBS concrete has demonstrated particular advantages in marine environments, such as bridge structures in Norwegian coastal regions[13], where its enhanced chloride-binding capacity and reduced permeability, when properly cured, significantly improve resistance to chloride-induced corrosion, as discussed in Section "How to evaluate the durabilityperformance of HVBSC?". These properties make HVBSC well-suited for use in coastal infrastructure such as bridges and seawalls. However, to fully realise the potential of HVBSCs and ensure consistent performance across diverse applications, several critical challenges must be addressed.

Figure 5 outlines the conceptual framework for the development of HVBSC integrating experimental, computational, and practical pathways to optimise early-age properties and long-term durability. A primary challenge is the extended setting time and slow reaction rate compared to conventional Portland cements, when the slag replacements is higher than 60 wt.%. This is largely attributed to the lower reactivity of slag and the reduced cement content[51,68]. To mitigate these issues, the application of filler

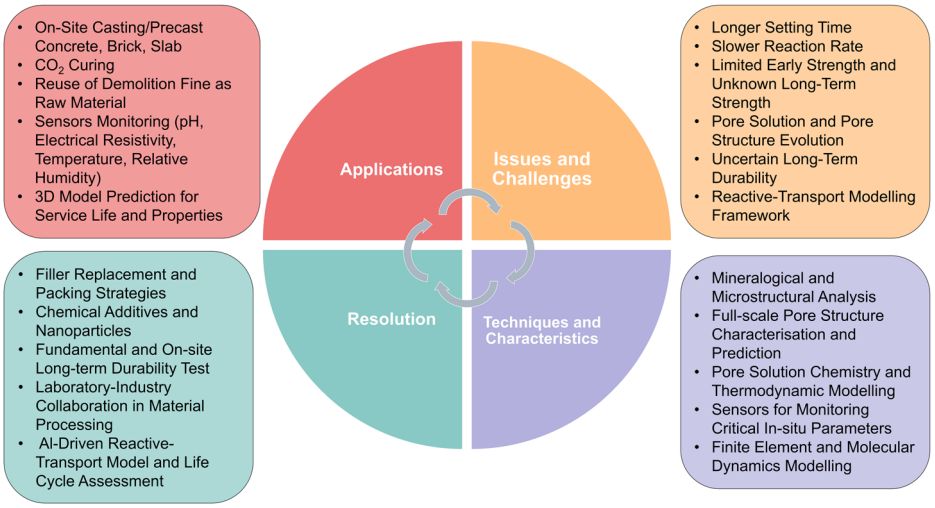

Fig. 5 | Conceptual framework illustrating the key issues and challenges associated with high-volume blended slag cement, characterisation techniques and modelling strategies, potential resolutions, and applications.

replacement strategies with optimised packing can enhance the particle size distribution in mix designs. This approach could be made feasible through collaboration with the cement industry, leveraging existing grinding technologies with minimal re-engineering[157,158]. This optimisation would also facilitate the incorporation of HVBSC into the circular economy as recycled aggregate when HVBSC is demolished after completing its service life[159,160], extending the lifecycle of these materials and enhancing sustainability from cradle to grave. Additionally, the judicious use of chemical additives and nanoparticles, such as C-S-H seeds, can accelerate hydration and improve early strength, although challenges such as low reactivity at ambient temperatures and potential nanoparticle agglomeration must be addressed to maintain workability.

The evolution of pore structure as a function of slag content and curing time is another critical factor, influencing the tortuosity and diffusivity of the pore network[161], which in turn governs mass transport and long-term durability in HVBSC. Increased slag content tends to refine gel pores, transitioning from a fibrillary to foil-like morphology[56]. shown in Fig. 3; however, large capillaries and macropores (greater than 50 nm) may proliferate due to a lower degree of reaction. Advanced non-destructive techniques like micro/nano computed tomography[162,163] offer promising avenues for reconstructing the 3D pore structure of cementitious materials, and scale-bridging algorithms[164,165] hold the potential to reconstruct pore networks across nanometre to millimetre scales.

Further fundamental studies on pore solution chemistry and thermodynamic modelling are crucial. As discussed in Sections "Reaction mechanism of high-volume blended slag cements"–"Microstructure evolution and mechanical properties", the current limitations in the thermodynamic database for C-(A)-S-H gel impede accurate evaluation of the Al substitution ratio in silicon tetrahedra. Integrating full-scale pore structure data with advanced thermodynamic modelling could enable the development of a 3D reactive-transport modelling framework, a significant milestone largely unexplored in cement and concrete. Coupled with machine learning[165,166], especially in correlating the chemical composition of raw materials with mechanical properties and durability, this framework could revolutionise material performance prediction under diverse conditions, facilitate spatially resolved CO_2 sequestration assessments, and ultimately contribute to the development of resilient and sustainable infrastructure with self-validating outcomes for policymakers.

In addition to overcoming technical challenges, the future of HVBSC hinges on continued innovation in material processing and the integration of sustainable practices. Collaboration between academic research and industry will be critical for scaling HVBSC production and ensuring effective deployment in large-scale construction projects. Moreover, exploring alternative materials and additives, such as graphene-based materials and carbon nanotubes, despite being in the research phase, could further enhance the performance and sustainability of HVBSC. However, the higher costs associated with these advanced materials remain a barrier to their widespread adoption in a cost-sensitive industry.

In conclusion, the prospects for advancing sustainability and standardisation in HVBSC are promising, yet they require a concerted effort from researchers, industry professionals, and policymakers. By addressing current challenges through innovative material design, advanced reactive-transport modelling, and the establishment of robust standards, HVBSC can significantly contribute to the transition towards more sustainable and durable construction practices. The proposed conceptual framework highlights the need for a multidisciplinary approach, combining insights from materials science, engineering, and environmental studies to fully unlock the potential of HVBSC.

Data availability

No datasets were generated or analysed during the current study.

Received: 12 September 2024; Accepted: 19 June 2025;
Published online: 05 August 2025

References

1. Monteiro, P. J. M., Miller, S. A. & Horvath, A. Towards sustainable concrete. *Nat. Mater.* **16**, 698–699 (2017).
2. Malhotra, V. Global warming, and role of supplementary cementing materials and superplasticisers in reducing greenhouse gas emissions from the manufacturing of portland cement. *Int. J. Struct. Eng.* **1**, 116–130 (2010).
3. Zhao, X., Ma, X., Chen, B., Shang, Y. & Song, M. Challenges toward carbon neutrality in China: Strategies and countermeasures. *Resour., Conserv. Recycling* **176**, 105959 (2022).
4. Zhu, J. & Chertow, M. R. Greening industrial production through waste recovery: "Comprehensive utilization of resources" in China. *Environ. Sci. Technol.* **50**, 2175–2182 (2016).
5. Zeng, H. et al. Progress on the industrial applications of red mud with a focus on China. *Minerals* **10**, 773 (2020).
6. Zeng, N. et al. The Chinese carbon-neutral goal: challenges and prospects. *Adv. Atmos. Sci.* **39**, 1229–1238 (2022).
7. He, J. et al. Towards carbon neutrality: a study on China's long-term low-carbon transition pathways and strategies. *Environ. Sci. Ecotechnol.* **9**, 100134 (2022).
8. Jaysawal, D. N. & Saha, S. Urbanization in India: An impact assessment. *Int. J. Appl. Sociol.* **4**, 60–65 (2014).
9. Mohammadi, A. & Ramezanianpour, A. M. Investigating the environmental and economic impacts of using supplementary

cementitious materials (SCMs) using the life cycle approach. *J. Build. Eng.* **79**, 107934 (2023).
10. Crossin, E. The greenhouse gas implications of using ground granulated blast furnace slag as a cement substitute. *J. Clean. Prod.* **95**, 101–108 (2015).
11. Matthes, W. et al. Ground granulated blast-furnace slag, properties of fresh and hardened concrete containing supplementary cementitious materials: State-of-the-art report of the RILEM technical committee 238-SCM. *Working Group* **4**, 1–53 (2018).
12. Blankendaal, T., Schuur, P. & Voordijk, H. Reducing the environmental impact of concrete and asphalt: a scenario approach. *J. Clean. Prod.* **66**, 27–36 (2014).
13. Gjørv O.E., Durability design of concrete structures in severe environments (2nd ed.), CRC Press (2014).
14. Ting K.H., Tropical green building rating systems: A comparison between Green Building Index and BCA Green Mark, 2012 IEEE Business, Engineering & Industrial Applications Colloquium (BEIAC), IEEE, 2012, pp. 263-268.
15. Kubba S., LEED practices, certification, and accreditation handbook, Butterworth-Heinemann (2009).
16. Sanjuán, M. & Argiz, C. The new European standard on common cements specifications EN 197-1: 2011. *Materiales de. Construcción* **62**, 425–430 (2012).
17. Blotevogel, S. et al. Ability of the R^3 test to evaluate differences in early age reactivity of 16 industrial ground granulated blast furnace slags (GGBS). *Cem. Concr. Res.* **130**, 105998 (2020).
18. Yang, K. et al. First structural use of site-cast, alkali-activated slag concrete in China. *Proc. Inst. Civ. Eng. - Struct. Build.* **171**, 800–809 (2018).
19. Provis J.L., et al., Demonstration projects and applications in building and civil infrastructure, Alkali Activated Materials: State-of-the-Art Report, RILEM TC 224-AAM, (2014) 309-338.
20. Zou, J., Liu, Z. & Guo, Q. Comprehensive utilisation of blast furnace slag. *Can. Metall. Q.* **63**, 927–934 (2024).
21. J.G. Peacey, W.G. Davenport, The iron blast furnace: theory and practice, Elsevier (2016).
22. Jiang, Y., Ling, T.-C., Shi, C. & Pan, S.-Y. Characteristics of steel slags and their use in cement and concrete—A review. *Resour., Conserv. Recycling* **136**, 187–197 (2018).
23. Buddhdev, B. G. & Timani, K. L. Critical review for utilization of blast furnace slag in geotechnical application. *Problematic Soils Geoenviron. Concerns: Proc. IGC* **2018**, 87–98 (2020).
24. J. Liu, D. Wang, Application of ground granulate blast furnace slag-steel slag composite binder in a massive concrete structure under severe sulphate attack, *Adv. Mater. Sci. Eng.*, 2017 9493043 (2017).
25. Buddhdev, B. & Varia, H. Feasibility study on application of blast furnace slag in pavement concrete. *Int. J. Innov. Res. Sci., Eng. Technol.* **3**, 10795–10802 (2014).
26. Carlsson B. The West European Steel Industry Structure and Competitiveness in Historical Perspective, IUI Working Paper, (1980).
27. Faremo, G. Build resilient infrastructure, promote inclusive and sustainable industrialization and foster innovation. *UN Chron.* **51**, 21–22 (2015).
28. Han, F., Zhang, Z., Wang, D. & Yan, P. Hydration heat evolution and kinetics of blended cement containing steel slag at different temperatures. *Thermochim. Acta* **605**, 43–51 (2015).
29. Shi, C. Steel slag—its production, processing, characteristics, and cementitious properties. *J. Mater. Civ. Eng.* **16**, 230–236 (2004).
30. Huaiwei, Z. & Xin, H. An overview for the utilization of wastes from stainless steel industries. *Resour. Conserv. Recycling* **55**, 745–754 (2011).
31. Adu-Amankwah, S., Zajac, M., Stabler, C., Lothenbach, B. & Black, L. Influence of limestone on the hydration of ternary slag cements. *Cem. Concr. Res.* **100**, 96–109 (2017).
32. Durdziński, P. T., Ben Haha, M., Zajac, M. & Scrivener, K. L. Phase assemblage of composite cements. *Cem. Concr. Res.* **99**, 172–182 (2017).
33. Paul, M. & Glasser, F. Impact of prolonged warm (85 °C) moist cure on Portland cement paste. *Cem. Concr. Res.* **30**, 1869–1877 (2000).
34. Le Saout, G., Lécolier, E., Rivereau, A. & Zanni, H. Chemical structure of cement aged at normal and elevated temperatures and pressures: Part I. Class G oilwell cement. *Cem. Concr. Res.* **36**, 71–78 (2006).
35. Dilnesa, B., Wieland, E., Lothenbach, B., Dähn, R. & Scrivener, K. Fe-containing phases in hydrated cements. *Cem. Concr. Res.* **58**, 45–55 (2014).
36. Damidot, D. & Glasser, F. Investigation of the CaO-Al_2O_3-SiO_2-H_2O system at 25 °C by thermodynamic calculations. *Cem. Concr. Res.* **25**, 22–28 (1995).
37. Ding, J., Fu, Y. & Beaudoin, J. Strätlingite formation in high alumina cement-silica fume systems: significance of sodium ions. *Cem. Concr. Res.* **25**, 1311–1319 (1995).
38. Winnefeld, F. & Lothenbach, B. Hydration of calcium sulfoaluminate cements—Experimental findings and thermodynamic modelling. *Cem. Concr. Res.* **40**, 1239–1247 (2010).
39. Dodson V.H., Pozzolans and the pozzolanic reaction, Concrete admixtures, Springer, 159-201 (1990).
40. Grattan-Bellew, P. Microstructural investigation of deteriorated Portland cement concretes. *Constr. Build. Mater.* **10**, 3–16 (1996).
41. Taylor, R., Richardson, I. & Brydson, R. Composition and microstructure of 20-year-old ordinary Portland cement–ground granulated blast-furnace slag blends containing 0 to 100% slag,. *Cem. Concr. Res.* **40**, 971–983 (2010).
42. Zhu, X., Luan, M., Tang, D., Yang, K. & Yang, C. Understanding the setting behaviours of alkali-activated slag from the dissolution-precipitation point of view. *Cem. Concr. Compos.* **148**, 105474 (2024).
43. Zhu, X., Zhang, Z., Luan, M., Yang, K. & Li, J. Temperature-sensitively dissolving of GGBS in neutral and alkali media. *Constr. Build. Mater.* **418**, 135353 (2024).
44. Zhu, X., Zhang, M., Yang, K., Yu, L. & Yang, C. Setting behaviours and early-age microstructures of alkali-activated ground granulated blast furnace slag (GGBS) from different regions in China. *Cem. Concr. Compos.* **114**, 103782 (2020).
45. Ogirigbo, O. R. & Black, L. Influence of slag composition and temperature on the hydration and microstructure of slag blended cements. *Constr. Build. Mater.* **126**, 496–507 (2016).
46. Kumar, S. et al. Mechanical activation of granulated blast furnace slag and its effect on the properties and structure of portland slag cement. *Cem. Concr. Compos.* **30**, 679–685 (2008).
47. Gu, X. et al. Synergistic effect and mechanism of lithium slag on mechanical properties and microstructure of steel slag-cement system. *Constr. Build. Mater.* **396**, 131768 (2023).
48. Avet, F., Snellings, R., Diaz, A. A., Haha, M. B. & Scrivener, K. Development of a new rapid, relevant and reliable (R3) test method to evaluate the pozzolanic reactivity of calcined kaolinitic clays. *Cem. Concr. Res.* **85**, 1–11 (2016).
49. Londono-Zuluaga, D. et al. Report of RILEM TC 267-TRM phase 3: validation of the R3 reactivity test across a wide range of materials. *Mater. Struct.* **55**, 142 (2022).
50. A. C1897-20, Standard Test Methods for Measuring the Reactivity of Supplementary Cementitious Materials by Isothermal Calorimetry and Bound Water Measurements, ASTM C, 2020, 5.
51. Lumley, J., Gollop, R., Moir, G. & Taylor, H. Degrees of reaction of the slag in some blends with Portland cements. *Cem. Concr. Res.* **26**, 139–151 (1996).
52. Blotevogel, S. et al. Glass structure of industrial ground granulated blast furnace slags (GGBS) investigated by time-resolved Raman and NMR spectroscopies. *J. Mater. Sci.* **56**, 17490–17504 (2021).

53. Stebbins, J. F. & Xu, Z. NMR evidence for excess non-bridging oxygen in an aluminosilicate glass. *Nature* **390**, 60–62 (1997).
54. Marsh, A. T. et al. Influence of limestone addition on sodium sulphate activated blast furnace slag cements. *Constr. Build. Mater.* **360**, 129527 (2022).
55. Herterich, J., Richardson, I., Moro, F., Marchi, M. & Black, L. Microstructure and phase assemblage of low-clinker cements during the early stages of carbonation. *Cem. Concr. Res.* **152**, 106643 (2022).
56. Zhu, X. & Richardson, I. G. Morphology-structural change of C-A-S-H gel in blended cements. *Cem. Concr. Res.* **168**, 107156 (2023).
57. Richardson, I., Girão, A., Taylor, R. & Jia, S. Hydration of water-and alkali-activated white Portland cement pastes and blends with low-calcium pulverized fuel ash. *Cem. Concr. Res.* **83**, 1–18 (2016).
58. Richardson, I. G. Model structures for C-(A)-S-H (I). *Acta Crystallogr. Sect. B: Struct. Sci., Cryst. Eng. Mater.* **70**, 903–923 (2014).
59. Chaouche, M., Gao, X. X., Cyr, M., Cotte, M. & Frouin, L. On the origin of the blue/green color of blast-furnace slag-based materials: Sulfur K-edge XANES investigation. *J. Am. Ceram. Soc.* **100**, 1707–1716 (2017).
60. Arai, Y., Powell, B. A. & Kaplan, D. I. Sulfur speciation in untreated and alkali treated ground-granulated blast furnace slag. *Sci. Total Environ.* **589**, 117–121 (2017).
61. Richardson, I. & Groves, G. Microstructure and microanalysis of hardened cement pastes involving ground granulated blast-furnace slag. *J. Mater. Sci.* **27**, 6204–6212 (1992).
62. Klemczak, B. & Batog, M. Heat of hydration of low-clinker cements: Part I. Semi-adiabatic and isothermal tests at different temperature. *J. Therm. Anal. Calorim.* **123**, 1351–1360 (2016).
63. Gruyaert, E., Robeyst, N. & De, B. N. Study of the hydration of Portland cement blended with blast-furnace slag by calorimetry and thermogravimetry. *J. Therm. Anal. Calorim.* **102**, 941–951 (2010).
64. Hosan, A. & Shaikh, F. U. A. Compressive strength development and durability properties of high volume slag and slag-fly ash blended concretes containing nano-CaCO3. *J. Mater. Res. Technol.* **10**, 1310–1322 (2021).
65. Bougara, A., Lynsdale, C. & Milestone, N. B. The influence of slag properties, mix parameters and curing temperature on hydration and strength development of slag/cement blends. *Constr. Build. Mater.* **187**, 339–347 (2018).
66. Bilim, C., Atiş, C. D., Tanyildizi, H. & Karahan, O. Predicting the compressive strength of ground granulated blast furnace slag concrete using artificial neural network. *Adv. Eng. Softw.* **40**, 334–340 (2009).
67. Etcheverry, J. M. et al. Phase Evolution of Hybrid Alkali Sulfate-Activated Ground-Granulated Blast Furnace Slag Cements. *ACS Sustain. Chem. Eng.* **11**, 17519–17531 (2023).
68. Kolani, B. et al. Hydration of slag-blended cements. *Cem. Concr. Compos.* **34**, 1009–1018 (2012).
69. Snellings, R. Solution-controlled dissolution of supplementary cementitious material glasses at pH 13: the effect of solution composition on glass dissolution rates. *J. Am. Ceram. Soc.* **96**, 2467–2475 (2013).
70. Suraneni, P., Palacios, M. & Flatt, R. J. New insights into the hydration of slag in alkaline media using a micro-reactor approach. *Cem. Concr. Res.* **79**, 209–216 (2016).
71. Richardson, I. G., Brough, A. R., Brydson, R., Groves, G. W. & Dobson, C. M. Location of aluminum in substituted calcium silicate hydrate (C-S-H) gels as determined by 29Si and 27Al NMR and EELS. *J. Am. Ceram. Soc.* **76**, 2285–2288 (1993).
72. Andersen, M. D., Jakobsen, H. J. & Skibsted, J. Incorporation of aluminum in the calcium silicate hydrate (C− S− H) of hydrated Portland cements: A high-field 27Al and 29Si MAS NMR investigation. *Inorg. Chem.* **42**, 2280–2287 (2003).
73. Sun, G., Young, J. F. & Kirkpatrick, R. J. The role of Al in C–S–H: NMR, XRD, and compositional results for precipitated samples. *Cem. Concr. Res.* **36**, 18–29 (2006).
74. Double, D., Hellawell, A. & Perry, S. The hydration of Portland cement. *Proc. R. Soc. Lond. A. Math. Phys. Sci.* **359**, 435–451 (1978).
75. Richardson, I. G. The nature of CSH in hardened cements. *Cem. Concr. Res.* **29**, 1131–1147 (1999).
76. Richardson, I. G., Brough, A. R., Groves, G. W. & Dobson, C. M. The characterization of hardened alkali-activated blast-furnace slag pastes and the nature of the calcium silicate hydrate (C-S-H) phase. *Cem. Concr. Res.* **24**, 813–829 (1994).
77. Richardson, I. & Li, S. Composition and structure of an 18-year-old 5M KOH-activated ground granulated blast-furnace slag paste. *Constr. Build. Mater.* **168**, 404–411 (2018).
78. Ke, X., Criado, M., Provis, J. L. & Bernal, S. A. Slag-based cements that resist damage induced by carbon dioxide. *ACS Sustain. Chem. Eng.* **6**, 5067–5075 (2018).
79. Ke, X., Bernal, S. A., Provis, J. L. & Lothenbach, B. Thermodynamic modelling of phase evolution in alkali-activated slag cements exposed to carbon dioxide. *Cem. Concr. Res.* **136**, 106158 (2020).
80. Liu, X., Lu, S., Tang, Z., Wang, Z. & Huang, T. Removal of sulfate from aqueous solution using Mg–Al nano-layered double hydroxides synthesized under different dual solvent systems. *Nanotechnol. Rev.* **10**, 117–125 (2021).
81. Ke, X., Bernal, S. A., Hussein, O. H. & Provis, J. L. Chloride binding and mobility in sodium carbonate-activated slag pastes and mortars. *Mater. Struct.* **50**, 252 (2017).
82. Liu T., Chen Y., Yu Q., Brouwers H.J., Effect of MgO, nitrate intercalated LDH and Calcined-LDH on chloride resistance of alkali-activated fly ash/slag mortar, 2nd International Conference of Sustainable Building Materials (ICSBM 2019), (2019).
83. Zhang, J. et al. Effects of Mg-based admixtures on chloride diffusion in alkali-activated fly ash-slag mortars. *Case Stud. Constr. Mater.* **21**, e03659 (2024).
84. Richardson, I. G. The importance of proper crystal-chemical and geometrical reasoning demonstrated using layered single and double hydroxides. *Acta Crystallogr. Sect. B: Struct. Sci., Cryst. Eng. Mater.* **69**, 150–162 (2013).
85. Prentice, D. P. et al. The effects of (di-, tri-valent)-cation partitioning and intercalant anion-type on the solubility of hydrotalcites. *J. Am. Ceram. Soc.* **103**, 6025–6039 (2020).
86. Bernard, E., Zucha, W. J., Lothenbach, B., & Mäder, U. Stability of hydrotalcite (Mg-Al layered double hydroxide) in presence of different anions. *Cem. Concr. Res.* **152**, 106674 (2022).
87. Scrivener, K. L. Backscattered electron imaging of cementitious microstructures: understanding and quantification. *Cem. Concr. Compos.* **26**, 935–945 (2004).
88. D.G. Evans, R.C. Slade, Structural aspects of layered double hydroxides, Layered double hydroxides 1-87 (2006).
89. Skibsted, J., Henderson, E. & Jakobsen, H. J. Characterization of calcium aluminate phases in cements by aluminum-27 MAS NMR spectroscopy. *Inorg. Chem.* **32**, 1013–1027 (1993).
90. Haha, M. B., Lothenbach, B., Le Saout, G. & Winnefeld, F. Influence of slag chemistry on the hydration of alkali-activated blast-furnace slag—Part I: Effect of MgO. *Cem. Concr. Res.* **41**, 955–963 (2011).
91. Z. Yue, Y. Dhandapani, S. Adu-Amankwah, S.A. Bernal, Phase evolution and performance of sodium sulfate-activated slag cement pastes, Cement 100117, (2024).
92. Ke, X., Bernal, S. A. & Provis, J. L. Controlling the reaction kinetics of sodium carbonate-activated slag cements using calcined layered double hydroxides. *Cem. Concr. Res.* **81**, 24–37 (2016).
93. Zhang, L. & Chen, B. Hydration and properties of slag cement activated by alkali and sulfate. *J. Mater. Civ. Eng.* **29**, 04017091 (2017).

94. Alzaza, A., Ohenoja, K., Dabbebi, R. & Illikainen, M. Enhancing the hardened properties of blended cement paste cured at 0 °C by using alkali-treated ground granulated blast furnace slag. *Cem. Concr. Compos.* **134**, 104757 (2022).
95. Thymotie A., Chang T., Nguyen H., Effect of sodium silicate as activator on the fresh and hardened properties of cement-slag blended paste, IOP Conference Series: Materials Science and Engineering, IOP Publishing, 012116 (2019).
96. Fu, J. et al. Mechanisms of enhancement in early hydration by sodium sulfate in a slag-cement blend–Insights from pore solution chemistry. *Cem. Concr. Res.* **135**, 106110 (2020).
97. Sun, H., Qian, J., Yang, Y., Fan, C. & Yue, Y. Optimization of gypsum and slag contents in blended cement containing slag. *Cem. Concr. Compos.* **112**, 103674 (2020).
98. Singh, M. Influence of blended gypsum on the properties of Portland cement and Portland slag cement. *Cem. Concr. Res.* **30**, 1185–1188 (2000).
99. Wu, Y., Duan, P. & Yan, C. Role of layered double hydroxides in setting, hydration degree, microstructure and compressive strength of cement paste. *Appl. Clay Sci.* **158**, 123–131 (2018).
100. Shui, Z. H. et al. Improvement of concrete carbonation resistance based on a structure modified Layered Double Hydroxides (LDHs): Experiments and mechanism analysis. *Constr. Build. Mater.* **176**, 228–240 (2018).
101. Seifu, M. N., Jang, D., Kim, G. M. & Park, S. Improving properties of Portland cement-blast furnace slag blended paste through sodium bicarbonate-induced carbonation. *Dev. Built Environ.* **20**, 100575 (2024).
102. Zunino, F. & Scrivener, K. Factors influencing the sulfate balance in pure phase C3S/C3A systems. *Cem. Concr. Res.* **133**, 106085 (2020).
103. Zunino, F. & Scrivener, K. Insights on the role of alumina content and the filler effect on the sulfate requirement of PC and blended cements. *Cem. Concr. Res.* **160**, 106929 (2022).
104. Zunino, F. & Scrivener, K. The influence of the filler effect on the sulfate requirement of blended cements. *Cem. Concr. Res.* **126**, 105918 (2019).
105. Soroka, I. & Setter, N. The effect of fillers on strength of cement mortars. *Cem. Concr. Res.* **7**, 449–456 (1977).
106. John, V. M., Damineli, B. L., Quattrone, M. & Pileggi, R. G. Fillers in cementitious materials—Experience, recent advances and future potential. *Cem. Concr. Res.* **114**, 65–78 (2018).
107. Berodier, E. & Scrivener, K. Understanding the filler effect on the nucleation and growth of C-S-H. *J. Am. Ceram. Soc.* **97**, 3764–3773 (2014).
108. Ouyang, X., Koleva, D., Ye, G. & Van, K. Breugel, Understanding the adhesion mechanisms between CSH and fillers. *Cem. Concr. Res.* **100**, 275–283 (2017).
109. Wang, D. et al. A review on use of limestone powder in cement-based materials: Mechanism, hydration and microstructures. *Constr. Build. Mater.* **181**, 659–672 (2018).
110. Georget, F., Lothenbach, B., Wilson, W., Zunino, F. & Scrivener, K. L. Stability of hemicarbonate under cement paste-like conditions. *Cem. Concr. Res.* **153**, 106692 (2022).
111. Adu-Amankwah, S., Lopez, S. A. B. & Black, L. Influence of component fineness on hydration and strength development in ternary slag-limestone cements. *RILEM Tech. Lett.* **4**, 81–88 (2019).
112. De Larrard F., Concrete mixture proportioning: a scientific approach, CRC Press (1999).
113. Riding, K., Silva, D. A. & Scrivener, K. Early age strength enhancement of blended cement systems by CaCl2 and diethanol-isopropanolamine. *Cem. Concr. Res.* **40**, 935–946 (2010).
114. Justnes, H., Danner, T. & Torabzadegan, M. Effect of calcium nitrate on the performance of slag blended cement. *Adv. Sci. Technol.* **145**, 45–54 (2024).
115. Li, X., Bizzozero, J. & Hesse, C. Impact of CSH seeding on hydration and strength of slag blended cement. *Cem. Concr. Res.* **161**, 106935 (2022).
116. Xu, C., Li, H. & Yang, X. Effect and characterization of the nucleation CSH seed on the reactivity of granulated blast furnace slag powder. *Constr. Build. Mater.* **238**, 117726 (2020).
117. Land, G. & Stephan, D. The effect of synthesis conditions on the efficiency of C-S-H seeds to accelerate cement hydration. *Cem. Concr. Compos.* **87**, 73–78 (2018).
118. Li, J., Zhang, W., Xu, K. & Monteiro, P. J. M. Fibrillar calcium silicate hydrate seeds from hydrated tricalcium silicate lower cement demand. *Cem. Concr. Res.* **137**, 106195 (2020).
119. Feng, Q., Mao, Y., Peng, Z., Zheng, Y. & Wu, J. Preparation and properties of low-temperature early strength material for nano-C-S-H gel seed. *Arab. J. Sci. Eng.* **47**, 5567–5575 (2022).
120. Pedrosa, H. C. et al. Hydration of Portland cement accelerated by C-S-H seeds at different temperatures. *Cem. Concr. Res.* **129**, 105978 (2020).
121. Kutschera M., Nicoleau L., Bräu M., Nano-optimized construction materials by nano-seeding and crystallization control, Nanotechnology in Civil Infrastructure: A Paradigm Shift, Springer, 175-205 (2011).
122. Jing, G. et al. Introducing reduced graphene oxide to enhance the thermal properties of cement composites. *Cem. Concr. Compos.* **109**, 103559 (2020).
123. Yang, H. et al. A critical review on research progress of graphene/cement based composites. *Compos. Part A: Appl. Sci. Manuf.* **102**, 273–296 (2017).
124. Rashad, A. M. Effect of carbon nanotubes (CNTs) on the properties of traditional cementitious materials. *Constr. Build. Mater.* **153**, 81–101 (2017).
125. Alex, A. G., Kedir, A. & Tewele, T. G. Review on effects of graphene oxide on mechanical and microstructure of cement-based materials. *Constr. Build. Mater.* **360**, 129609 (2022).
126. Tarpani, R. R. Z. et al. Environmental assessment of cement production with added graphene. *Clean. Environ. Syst.* **14**, 100206 (2024).
127. Zhang, Q., Huang, J. Q., Qian, W. Z., Zhang, Y. Y. & Wei, F. The road for nanomaterials industry: A review of carbon nanotube production, post-treatment, and bulk applications for composites and energy storage. *small* **9**, 1237–1265 (2013).
128. Wen, L., Li, F. & Cheng, H. M. Carbon nanotubes and graphene for flexible electrochemical energy storage: from materials to devices. *Adv. Mater.* **28**, 4306–4337 (2016).
129. Wang, J., Xu, Y., Wu, X., Zhang, P. & Hu, S. Advances of graphene- and graphene oxide-modified cementitious materials. *Nanotechnol. Rev.* **9**, 465–477 (2020).
130. Murali, M. et al. Utilizing graphene oxide in cementitious composites: A systematic review. *Case Stud. Constr. Mater.* **17**, e01359 (2022).
131. Thomas, M. D. A. & Bamforth, P. B. Modelling chloride diffusion in concrete: Effect of fly ash and slag. *Cem. Concr. Res.* **29**, 487–495 (1999).
132. Al-Amoudi, O. S. B. Attack on plain and blended cements exposed to aggressive sulfate environments. *Cem. Concr. Compos.* **24**, 305–316 (2002).
133. Al-Amoudi O., Mechanisms of sulfate attack in plain and blended cements: a review, Extending Performance of Concrete Structures: Proceedings of the International Seminar held at the University of Dundee, Scotland, UK on 7 September 1999, Thomas Telford Publishing, 247-260 (1999).
134. Hekal, E. E., Kishar, E. & Mostafa, H. Magnesium sulfate attack on hardened blended cement pastes under different circumstances. *Cem. Concr. Res.* **32**, 1421–1427 (2002).
135. Blotevogel, S. et al. The influence of Al_2O_3, CaO, MgO and TiO_2 content on the early-age reactivity of GGBS in blended cements,

alkali-activated materials and supersulfated cements. *Cem. Concr. Res.* **178**, 107439 (2024).
136. Zhang Y., The effect of blast furnace slag chemistry on carbonation characteristics of cement-slag systems, (2022).
137. Otieno, M., Beushausen, H. & Alexander, M. Effect of chemical composition of slag on chloride penetration resistance of concrete. *Cem. Concr. Compos.* **46**, 56–64 (2014).
138. Ogirigbo, O. R. & Black, L. The effect of slag composition and curing duration on the chloride ingress resistance of slag-blended cements. *Adv. Cem. Res.* **31**, 243–250 (2019).
139. Nosouhian, F. et al. Effects of slag characteristics on sulfate durability of Portland cement-slag blended systems. *Constr. Build. Mater.* **229**, 116882 (2019).
140. Whittaker M.J., The impact of slag composition on the microstructure of composite slag cements exposed to sulfate attack, University of Leeds, (2014).
141. Rao N.V., Meena T., A review on carbonation study in concrete, IOP Conference Series: Materials Science and Engineering, IOP Publishing, 032011, (2017).
142. von Greve-Dierfeld, S. et al. Understanding the carbonation of concrete with supplementary cementitious materials: a critical review by RILEM TC 281-CCC. *Mater. Struct.* **53**, 136 (2020).
143. Ngala, V. & Page, C. Effects of carbonation on pore structure and diffusional properties of hydrated cement pastes. *Cem. Concr. Res.* **27**, 995–1007 (1997).
144. Gruyaert, E., Van den Heede, P. & De Belie, N. Carbonation of slag concrete: Effect of the cement replacement level and curing on the carbonation coefficient–Effect of carbonation on the pore structure. *Cem. Concr. Compos.* **35**, 39–48 (2013).
145. Angst, U. et al. Corrosion of steel in carbonated concrete: mechanisms, practical experience, and research priorities–a critical review by RILEM TC 281-CCC. *RILEM Tech. Lett.* **5**, 85–100 (2020).
146. Yue, Z. et al. 3D crystalline phase and pore structure evolution upon CO_2 exposure in sodium sulfate-activated cement pastes. *Cem. Concr. Res.* **187**, 107716 (2025).
147. Seo, J., Park, S., Kim, G. M. & Park, S. Exploring natural and accelerated carbonation of alkali-activated slag. *Constr. Build. Mater.* **432**, 136459 (2024).
148. Liu, Z. et al. Carbonation of blast furnace slag concrete at different CO2 concentrations: Carbonation rate, phase assemblage, microstructure and thermodynamic modelling. *Cem. Concr. Res.* **169**, 107161 (2023).
149. Liu, W. et al. Changes in chemical phases and microscopic characteristics of fly ash blended cement pastes in different CO2 concentrations. *Constr. Build. Mater.* **257**, 119598 (2020).
150. Drouet, E., Poyet, S., Le Bescop, P., Torrenti, J.-M. & Bourbon, X. Carbonation of hardened cement pastes: Influence of temperature. *Cem. Concr. Res.* **115**, 445–459 (2019).
151. Xu, Z. et al. Effects of temperature, humidity and CO2 concentration on carbonation of cement-based materials: A review. *Constr. Build. Mater.* **346**, 128399 (2022).
152. Leemann, A. & Moro, F. Carbonation of concrete: the role of CO 2 concentration, relative humidity and CO 2 buffer capacity. *Mater. Struct.* **50**, 1–14 (2017).
153. Steiner, S., Lothenbach, B., Proske, T., Borgschulte, A. & Winnefeld, F. Effect of relative humidity on the carbonation rate of portlandite, calcium silicate hydrates and ettringite. *Cem. Concr. Res.* **135**, 106116 (2020).
154. Bernal, S. A. et al. Report of RILEM TC 281-CCC: A critical review of the standardised testing methods to determine carbonation resistance of concrete. *Mater. Struct.* **57**, 173 (2024).
155. Gluth, G. J. et al. Carbonation rate of alkali-activated concrete and high-volume SCM concrete: a literature data analysis by RILEM TC 281-CCC. *Mater. Struct.* **55**, 1–15 (2022).
156. von Greve-Dierfeld, S. et al. Understanding the carbonation of concrete with supplementary cementitious materials: a critical review by RILEM TC 281-CCC. *Mater. Struct.* **53**, 1–34 (2020).
157. Dvořák, K., Dolák, D. & Dočkal, J. Comparison of separate and co-grinding of the blended cements with the pozzolanic component. *Procedia Eng.* **151**, 66–72 (2016).
158. Öner, M. A study of intergrinding and separate grinding of blast furnace slag cement. *Cem. Concr. Res.* **30**, 473–480 (2000).
159. Colangelo, F., Navarro, T. G., Farina, I. & Petrillo, A. Comparative LCA of concrete with recycled aggregates: A circular economy mindset in Europe. *Int. J. Life Cycle Assess.* **25**, 1790–1804 (2020).
160. Perkins, L., Royal, A. C., Jefferson, I. & Hills, C. D. The use of recycled and secondary aggregates to achieve a circular economy within geotechnical engineering. *Geotechnics* **1**, 416–438 (2021).
161. Holzer L. et al. Tortuosity and microstructure effects in porous media: classical theories, empirical data and modern methods, Springer Nature (2023).
162. Bugani, S., Camaiti, M., Morselli, L., Van de Casteele, E. & Janssens, K. Investigation on porosity changes of Lecce stone due to conservation treatments by means of x-ray nano-and improved micro-computed tomography: preliminary results. *X-Ray Spectrom.: Int. J.* **36**, 316–320 (2007).
163. Withers, P. J. et al. X-ray computed tomography. *Nat. Rev. Methods Prim.* **1**, 18 (2021).
164. Karra, S. et al. Predictive scale-bridging simulations through active learning. *Sci. Rep.* **13**, 16262 (2023).
165. Lubbers, N. et al. Modeling and scale-bridging using machine learning: Nanoconfinement effects in porous media. *Sci. Rep.* **10**, 13312 (2020).
166. Y. Yan, Machine learning Fundamentals, Machine Learning in Chemical Safety and Health: Fundamentals with Applications 19-46 (2022).
167. C.N.B.o. Statistics, Industry Statistical Data (2025).
168. U.S.G. Survey, Minerals Yearbook-Metal and Minerals, (2025).
169. Statista, Global cement production (2025).
170. Cembureau, Activity Reports 2023, (2024).
171. E.S. Association, European Steel in Figures 2023, (2022).
172. Kulik, D. A. et al. GEM-Selektor geochemical modeling package: revised algorithm and GEMS3K numerical kernel for coupled simulation codes. *Comput. Geosci.* **17**, 1–24 (2013).
173. Wagner, T., Kulik, D. A., Hingerl, F. F. & Dmytrieva, S. V. GEM-Selektor geochemical modeling package: TSolMod library and data interface for multicomponent phase models. *Can. Mineralogist* **50**, 1173–1195 (2012).
174. Lothenbach, B. et al. Cemdata18: A chemical thermodynamic database for hydrated Portland cements and alkali-activated materials. *Cem. Concr. Res.* **115**, 472–506 (2019).
175. Lothenbach, B. & Winnefeld, F. Thermodynamic modelling of the hydration of Portland cement. *Cem. Concr. Res.* **36**, 209–226 (2006).
176. Taylor, H. F. Modification of the Bogue calculation. *Adv. Cem. Res.* **2**, 73–77 (1989).
177. Sajedi, F., Razak, H. A., Mahmud, H. B. & Shafigh, P. Relationships between compressive strength of cement–slag mortars under air and water curing regimes. *Constr. Build. Mater.* **31**, 188–196 (2012).
178. Yun, C. M., Rahman, M. R., Phing, C. Y. W., Chie, A. W. M. & Bakri, M. K. B. The curing times effect on the strength of ground granulated blast furnace slag (GGBFS) mortar. *Constr. Build. Mater.* **260**, 120622 (2020).
179. Xu, Z. et al. Hydration of blended cement with high-volume slag and nano-silica. *J. Build. Eng.* **64**, 105657 (2023).
180. Xu, Z. et al. Promoting utilization rate of ground granulated blast furnace slag (GGBS): Incorporation of nanosilica to improve the properties of blended cement containing high volume GGBS. *J. Clean. Prod.* **332**, 130096 (2022).

181. Guo, Z. et al. Synergistic effect of nanosilica and high-volume granulated blast furnace slag on pore structure and mechanical properties of cementitious materials. *J. Build. Eng.* **67**, 106003 (2023).

Acknowledgements
This research is sponsored by National Natural Science Fund for Excellent Young Scientists Fund Programme (Overseas) Grant: 23FAA02217 and the Young Scientists Fund of the National Natural Science Foundation of China (Grant No. 52408234). Z. Yue is sponsored and grateful to the China Postdoctoral Science Foundations (CPSF).

Author contributions
Z. Y. contributed to Conceptualization, Methodology, Investigation, Data curation, Formal analysis, Writing—original draft, Writing—review & editing. X. Z. contributed to Conceptualization, Methodology, Formal analysis, Funding acquisition, Supervision, Resources, Writing—original draft, Writing—review & editing.

Competing interests
The authors declare no competing interests.

Additional information
Correspondence and requests for materials should be addressed to Xiaohong Zhu.